

Variability Analysis in a 3-D Multi-Granular $\text{Hf}_x\text{Zr}_{1-x}\text{O}_2$ Ferroelectric Capacitor

Nilesh Pandey, Karishma Qureshi, and Yogesh Singh Chauhan

Abstract—A simulation-based study of variability of remnant polarization (P_r) in a multi-granular 3-D ultra-thin ferroelectric (FE) capacitor is presented in this paper. The Poisson Voronoi Tessellation Diagram (PVD) is used for the nucleation of grains in the FE region, which corresponds to the physical growth mechanism. The PVD algorithm implemented in MATLAB is coupled with TCAD simulations, to trace the ferroelectric hysteresis loop. It is found that the grains which have linear profile of P_r show larger variability in the FE hysteresis loop, compared to the grains, which follow the Gaussian distribution of P_r . Additionally, the impact of dielectric content in the FE grains is analyzed. It is seen that the dielectric grains cause very large amount of variability in the FE hysteresis loop. An increase in the dielectric grains also leads to a loss in the retentivity of the hysteresis loop.

Index Terms—Multi-Grain, Poisson Voronoi, Polycrystalline, dielectric phase, Preisach model.

I. INTRODUCTION

THE ferroelectric (FE) materials are being used extensively in the non-volatile memory (NVM) applications [1]- [4] and are also being explored for negative capacitance FET (NCFET) applications [5]- [21]. Ferroelectric crystal is most likely to grow in the poly-crystalline (multi-grain) form due to mismatch in lattice constants or defects in the process [22]- [28] and a fraction of ferroelectric grains always remains in the monoclinic phase, hence, these grains don't exhibit ferroelectricity [29], [30]. The locations of these monoclinic grains introduce an extra source of spatial variability in the remnant polarization (P_r) of NCFET [30]. In order to analyze the variability of remnant polarization with the dielectric (monoclinic) grains in the FE material, a Monte Carlo simulation-based study is proposed in [31]. Although the impact of dielectric grains on the FeFET NVM has been studied in [32], authors in [32] and other recent simulation-based studies [30], [31] consider the homogeneous square shape of grains and uniform FE properties in the whole grain, which is not practical. Because, the nucleation of grains in the FE region is completely random and depends on both size and position of the grain [22]- [28]. In this work, we develop a new methodology for the nucleation of grains to model the realistic experimental environment, which takes into account the dependence of nucleation on both the random shape and random position of grains.

This work was partially supported by the Swarna Jayanti Fellowship (Grant No. – DST/SJF/ETA-02/2017-18) and FIST Scheme (Grant No. – SR/FST/ETII-072/2016) of the Department of Science and Technology. N. Pandey, K. Qureshi and Y. S. Chauhan are with the Nanolab, Department of Electrical Engineering, IIT Kanpur, Kanpur 208016, India (e-mail: pandeyn@iitk.ac.in; chauhan@iitk.ac.in).

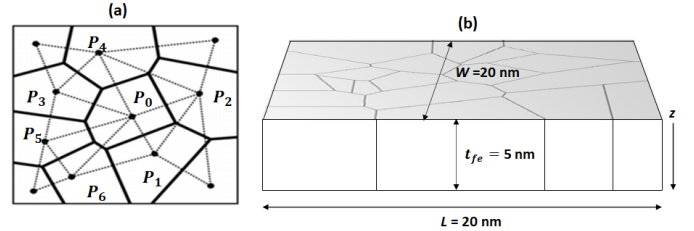


Fig. 1: (a) Grain distribution from PVD algorithm in a 2-D region where each polygon represents a grain of the FE material. (b) The grains are extruded in the z-direction to form 3-D columnar grains.

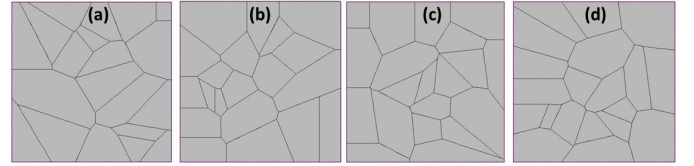


Fig. 2: A 2-D view of grains nucleated by PVD algorithm. The formation of grains in FE is random, hence, each figure shows a different grain pattern.

II. METHODOLOGY

First, defects points in the FE region are randomly scattered in a 2-D $x - y$ plane. Then Poisson Voronoi (PVD) algorithm [33], [34] is used to nucleate the grains by these defect points. Fig. 1(a) shows the implementation of PVD algorithm in a 2-D bounded region [34]. The points $P_0..P_6$ are randomly distributed and these points act as nucleation sites for the grains. Starting from an initial point (e.g. P_0), closest neighbor to this point are determined. Subsequently, perpendicular bisectors are drawn on dashed lines (joining lines of neighboring points) to form a closed polygon, which represent a grain. Since the size and the position of grains are randomly distributed in the FE region, to study the variability of P_r , 75 structures are considered in each simulation (beyond this sample of 75 structures, space replication is observed). Fig. 2 shows an example of the formation of grains in the FE. The nucleated grain is extruded along the z-axis until the FE thickness forms a 3-D grain structure (see Fig. 1(b)). Since the ferroelectric thickness is 5 nm, only one grain can be accommodated in the thickness direction [27], [28].

After the formation of 3-D PVD grains, the P_r is distributed into these grains. The FE grain structures are implemented in MATLAB [35], and these structures are used in 3-D Sentaurus TCAD [36], to capture the electrostatics of the device. A 3 V (peak to peak) and 100 Hz sinusoidal wave is applied at the input terminal of the FE capacitor and Preisach hysteresis model [37] is used to trace the FE hysteresis loop. The polar-

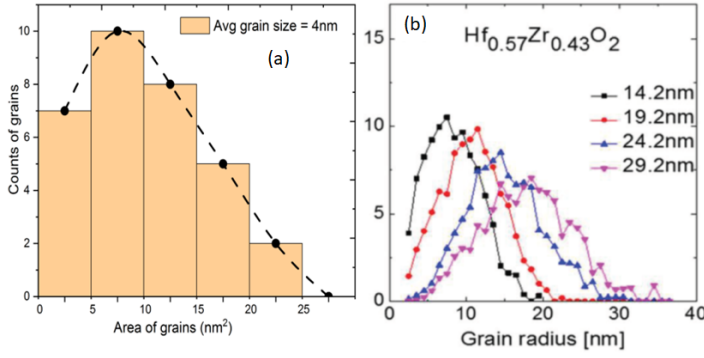


Fig. 3: (a) Distribution of grains with grain area follows the Gamma distribution. The area of each grain is calculated by MATLAB and the count of the grains (n) are given as, $n = 4(W \times L) / \pi (\text{grain size})^2$. (b) Demonstration of a Gamma distribution in the experimentally observed FE grains [24].

ization (P_r and P_s) are considered to be isotropic in all three coordinates axis. All other parameters in Preisach hysteresis model are taken to be their default values in TCAD Sentaurus [36]. It may be noted here that in the PVD algorithm, each grain is nucleated from a random defect point, which is also observed in the experimental results [22]- [28].

III. RESULTS AND DISCUSSION

A. Variability of P_r in Ferroelectric Grains

Fig. 3(a) shows the plot of number of grains (count of grains) with respect to the area of grains. It can be observed in the figure that grains distribution approximately follows the Gamma distribution profile. Fig. 3(b) shows the experimental results from [24], in which also grain distribution follows a gamma distribution profile, with average grain size of 4.3 nm. Thus, Fig. 3(a) and 3(b) show that the developed PVD algorithm closely matches with the experimental observations.

Experimental data, which shows direct dependence of P_r of $\text{Hf}_x\text{Zr}_{1-x}\text{O}_2$ (HZO) on the grain area is not available in the literature. However, the properties of FE material of class ABO_3 exhibit the size effect [25], [26]. The P_r of these materials varies linearly with grain area. Therefore, to study the variability of P_r of HZO material with respect to the grain area, we consider three different possibilities of P_r distribution: Gaussian, linearly increasing and linearly decreasing. Fig. 4 shows the polarization vs electric field (P-E) characteristic for the Gaussian distribution of P_r with respect to grain area. The median value of P_r is $27.67 \mu\text{C}/\text{cm}^2$ (P_r^m) [38], and the variance (σ), varies from $0.15 \times P_s$ to $0.35 \times P_s$. Hence, all the grains are allocated a different value of P_r within σ range. Total 75 samples of grain structures are considered for each σ simulation, and the results are plotted by taking the average of total simulated P-E loops. For smaller σ , the value of P_r of individual grain lies around the P_r^m . That is why, there is negligible change in P-E curves for small variations in σ . On the other hand, significant change is observed in the P-E loop, when σ approaches to $0.35P_s$.

Fig. 5(a) shows the 2-D surface plot of P_r versus grain area for linearly increasing P_r with grain area. First, we calculate the area of each grain. Then the value of P_r , that is

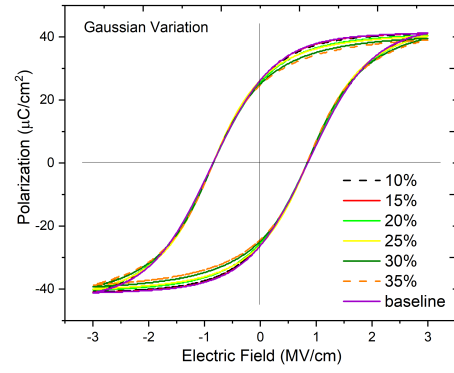


Fig. 4: Variability of P_r in the FE grains. The P_r follows the Gaussian distribution with the grain area. The variability is negligible in P-E loops for a smaller value of variance (σ). The variability is only observed for $\sigma \geq 30\%$.

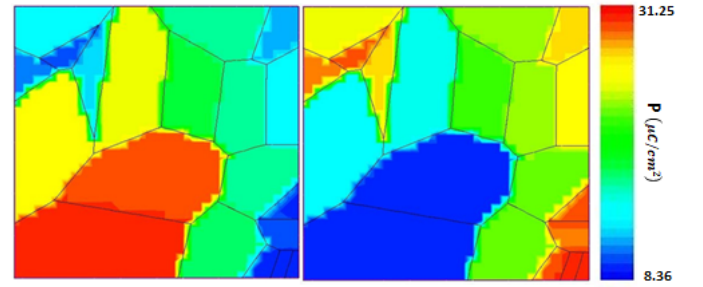


Fig. 5: 2-D surface distribution of P_r in FE grains. In (a) and (b), P_r is increasing and decreasing with the grains area respectively.

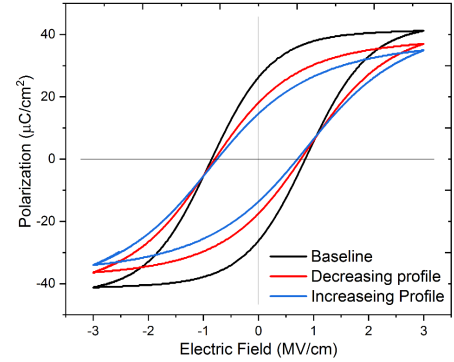


Fig. 6: Variability in the P-E hysteresis loop. The P_r is linearly increasing and decreasing with grain area. The linear dependency of P_r causes a much larger variability in P-E loop than the gaussian profile of P_r with grain area (see Fig. 4). The linear profile of P_r with the grain area is also observed in the experimental results as reported in [25], [26].

proportional to grain area is assigned to individual grain. Fig. 5(b) is plotted for linearly decreasing P_r with grain area. The same algorithm is used for all 75 different grain structures. The minimum value of P_r (P_r^{\min}) is $\approx 8 \mu\text{C}/\text{cm}^2$ considered [24], which corresponds to an undoped HZO ($\% \text{Zr} = 0$) ferroelectric and the maximum value of P_r (P_r^{\max}) is $31.25 \mu\text{C}/\text{cm}^2$ ($= 0.75P_s$).

Fig. 6 shows the variability in P-E loop for linearly increasing and linearly decreasing P_r with grain area, which is observed experimentally in the ABO_3 FE materials [25],

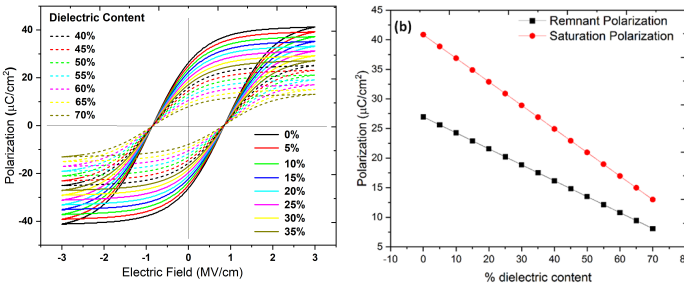


Fig. 7: (a) Impact of dielectric content in P-E hysteresis loop variability. (b) P_r and P_s variations with increasing dielectric content in the FE. As dielectric content increases in the FE material the P_r and P_s decreases which leads to a loss in the memory window of the FE capacitor.

[26]. It can be observed in Fig. 6 that the coercive field (E_c) reduces from 0.85 MV/cm to 0.7 MV/cm ($\approx 18\%$), which leads to reduction in the hysteresis loop. We can also see that polarization saturates to a lower value than baseline case. Here, the baseline stands for mono-grain FE, which has uniform property in the whole material. Additionally, the value of remnant polarization decreases by 47% compared to the baseline P_r . The red curve in Fig. 6 corresponds to linearly decreasing P_r with grain area. The values of P_r^{max} and P_r^{min} are assigned to grains, that have the smallest and largest area respectively (see Fig. 5(b)). The variability introduced by linear decreasing P_r (Red curve) is smaller than the linearly increasing P_r (Blue curve). That is why, for linearly decreasing E_c , P_r and P_s have values as 0.77 MV/cm, 18 $\mu\text{C}/\text{cm}^2$, and 37 $\mu\text{C}/\text{cm}^2$ respectively (smaller % change than Blue curve).

B. Dielectric Phase in Ferroelectric Grains

Some of the grains in the ferroelectric material do not exhibit the ferroelectricity and remain in dielectric phase [29]- [32]. To analyze the impact of dielectric content in FE, a linear relationship of polarization with the electric field ($P = \epsilon_0 (\epsilon_r + 1) E$, where, $\epsilon_r = 22$) is used in the specific percentage of total number of grains. The assigned maximum percentage to dielectric content is 70% of the total grains and the assigned minimum percentage is zero (pure FE material without any dielectric grains). In this work, we are simulating an isolated FE capacitor, hence, the positions of dielectric grains do not introduce any extra source of variability. Fig. 7(a) shows that as the dielectric content in the FE material increases, the P-E loops start to deteriorate and, hence, the ferroelectricity of the device starts to decrease. Fig. 7(b) shows the variations in P_r and P_s with dielectric content. Both decrease linearly with increment in the % of dielectric content in FE. The value of P_r approaches to that of baseline FE with % of Zr = 0, [24]) for dielectric content equal to the 60% in ferroelectric of total number of grains.

IV. CONCLUSION

The PVD algorithm is used to nucleate grains at randomly scattered defects points. Size and positions of nucleated grains are considered to be random in simulations. Hence, simulated results are remarkably close to the experimental observations.

We have shown that the variability in the P-E hysteresis loop is small for the Gaussian distribution of P_r with respect to grain area, due to small amount of variations in P_r of adjacent grains. However, variability in P-E loop increases significantly, when P_r follows the linear profile with respect to grain area. Additionally, both P_s decreases and hysteresis width reduces, hence, ferroelectricity (memory window) reduces. Therefore, experimentally fabricated FE device (which has variability of P_r in grains) will show poor retentivity than the mono-grain (uniform property in the whole material) FE device. Further, it is found that, the retentivity of FE memory decreases, as dielectric content in FE material increases.

REFERENCES

- [1] T. Sumi et al., "A 256 kb nonvolatile ferroelectric memory at 3 V and 100 ns," Proceedings of IEEE International Solid-State Circuits Conference - ISSCC '94, San Francisco, CA, USA, 1994, pp. 268-269, doi: 10.1109/ISSCC.1994.344646.
- [2] Wan S Y, Li Y, Li W, et al. Nonvolatile ferroelectric memory effect in ultrathin α - In_2Se_3 . *Adv Funct Mater*, 2018, 29, 1808606.
- [3] Huan Gao, Yuxi Yang, Yaojin Wang, Lang Chen, Junling Wang, Guoliang Yuan, and Jun-Ming Liu, "Transparent, Flexible, Fatigue-Free, Optical-Read, and Nonvolatile Ferroelectric Memories", *ACS Applied Materials & Interfaces* 2019 11 (38), 35169-35176 DOI: 10.1021/ac-sami.9b14095.
- [4] Wu, G., Tian, B., Liu, L. et al. Programmable transition metal dichalcogenide homojunctions controlled by nonvolatile ferroelectric domains. *Nat Electron* 3, 43–50 (2020). doi.org/10.1038/s41928-019-0350-y
- [5] S. Salahuddin and S. Datta, "Use of negative capacitance to provide voltage amplification for low power nanoscale devices," *Nano Lett.*, vol. 8, no. 2, pp. 405–410, 2007, doi: 10.1021/nl071804g.
- [6] G. A. Salvatore, D. Bouvet, and A. M. Ionescu, "Demonstration of subthreshold swing smaller than 60mV/decade in Fe-FET with P(VDF-TrFE)/ SiO_2 gate stack," in *IEDM Tech. Dig.*, Dec. 2008, pp. 1–4, doi: 10.1109/IEDM.2008.4796642.
- [7] C. W. Yeung, A. I. Khan, A. Sarker, S. Salahuddin, and C. Hu, "Low power negative capacitance FETs for future quantum-well body technology," in *Proc. Int. Symp. VLSI Technol., Syst., Appl. (VLSI-TSA)*, Apr. 2013, pp. 1–2, doi: 10.1109/VLSI-TSA.2013.6545648.
- [8] M. Kobayashi and T. Hiramoto, "Device design guideline for steep slope ferroelectric FET using negative capacitance in sub-0.2V operation: Operation speed, material requirement and energy efficiency," in *VLSI Symp. Tech. Dig.*, Jun. 2015, pp. T212–T213, doi: 10.1109/VLSIT.2015.7223678.
- [9] H. Ota, T. Ikegami, J. Hattori, K. Fukuda, S. Migita, A. Toriumi, "Fully coupled 3-D device simulation of negative capacitance FinFETs for sub 10 nm integration", *IEDM Tech. Dig.*, pp. 12.4.1-12.4.4, Dec. 2016, DOI: 10.1109/IEDM.2016.7838403
- [10] A. I. Khan, U. Radhakrishna, S. Salahuddin, and D. Antoniadis, "Work function engineering for performance improvement in leaky negative capacitance FETs," *IEEE Electron Device Lett.*, vol. 38, no. 9, pp. 1335–1338, Sep. 2017, DOI: 10.1109/LED.2017.2733382.
- [11] Cao, W., Banerjee, K. Is negative capacitance FET a steep-slope logic switch?, *Nat Commun* 11, 196 (2020). DOI: https://doi.org/10.1038/s41467-019-13797-9
- [12] V. P.-H. Hu, P.-C. Chiu, A. B. Sachid, and C. Hu, "Negative capacitance enables FinFET and FDSOI scaling to 2 nm node," in *Proc. Int. Electron Devices Meeting (IEDM)*, San Francisco, CA, USA, 2017, pp. 23.1.1–23.1.4, DOI: 10.1109/IEDM.2017.8268443.
- [13] N. Pandey and Y. S. Chauhan, "Analytical Modeling of Short-Channel Effects in MFIS Negative-Capacitance FET Including Quantum Confinement Effects," in *IEEE Transactions on Electron Devices*, vol. 67, no. 11, pp. 4757-4764, Nov. 2020, doi: 10.1109/TED.2020.3022002.
- [14] X. Zhang, X. Gong, and G. Liang, "Analysis on performance of ferroelectric NC-FETs based on real-space Gibbs-free energy with atomic channel structure," *IEEE Trans. Electron Devices*, vol. 66, no. 2, pp. 1100-1106, 2019.
- [15] Ku, Hansol, and Changhwan Shin. "Transient response of negative capacitance in P (VDF 0.75- TrFE 0.25) organic ferroelectric capacitor." *IEEE Journal of the Electron Devices Society* 5.3 (2017): 232-236.
- [16] Gao, W., Khan, A., Marti, X., Nelson, C., Serrao, C., Ravichandran, J., Ramesh, R. and Salahuddin, S., 2014. Room-temperature negative capacitance in a ferroelectric-dielectric superlattice heterostructure. *Nano letters*, 14(10), pp.5814-5819.
- [17] Appleby, Daniel JR, et al. "Experimental observation of negative capacitance in ferroelectrics at room temperature." *Nano letters* 14.7 (2014): 3864-3868.
- [18] Liu, S., Grinberg, I. and Rappe, A. Intrinsic ferroelectric switching from first principles. *Nature* 534, 360–363 (2016). https://doi.org/10.1038/nature18286.
- [19] A. K. Saha, P. Sharma, I. Dabo, S. Datta and S. K. Gupta, "Ferroelectric transistor model based on self-consistent solution of 2D Poisson's, non-equilibrium Green's function and multi-domain Landau Khalatnikov equations," 2017 IEEE International Electron Devices Meeting (IEDM), San Francisco, CA, 2017, pp. 13.5.1-13.5.4, doi: 10.1109/IEDM.2017.8268385.
- [20] A. Cano and D. Jiménez, "Multidomain ferroelectricity as a limiting factor for voltage amplification in ferroelectric field-effect transistors," *Appl. Phys. Lett.*, vol. 97, no. 13, p. 133509, 2010.
- [21] S. Kasamatsu, S. Watanabe, C. S. Hwang, and S. Han, "Emergence of negative capacitance in multidomain ferroelectric—Paraelectric nanocapacitors at finite bias," *Adv. Mater.*, vol. 28, no. 2, pp. 335–340, 2016.
- [22] Z. Zhao. et al, "Grain-Size Effects on the Ferroelectric Behavior of Dense Nanocrystalline BaTiO_3 Ceramics", DOI: 10.1103/PhysRevB.70.024107.
- [23] A. Dasgupta, P. Rastogi, D. Saha, A. Gaidhane, A. Agarwal and Y. S. Chauhan, "Modeling of Multi-domain Switching in Ferroelectric Materials: Application to Negative Capacitance FETs," 2018 IEEE International Electron Devices Meeting (IEDM), San Francisco, CA, 2018, pp. 9.2.1-9.2.4.
- [24] Park, M.H., et al (2017), "Surface and grain boundary energy as the key enabler of ferroelectricity in nanoscale hafnia-zirconia: a comparison of model and experiment. *Nanoscale*, 9 28, 9973-9986. https://doi.org/10.1039/C7NR02121F.
- [25] Tan, Y., Zhang, J., Wu, Y. et al. "Unfolding grain size effects in barium titanate ferroelectric ceramics". *Sci Rep* 5, 9953 (2015), — DOI: 10.1038/srep09953.
- [26] Mudinepalli, V.R., Feng, L., Lin, W. et al. Effect of grain size on dielectric and ferroelectric properties of nanostructured $\text{Ba}_{0.8}\text{Sr}_{0.2}\text{TiO}_3$ ceramics. *J Adv Ceram* 4, 46–53 (2015). https://doi.org/10.1007/s40145-015-0130-8.
- [27] S. J. Kim, J. Mohan, J. Lee, J. S. Lee, A. T. Lucero, C. D. Young, L. Colombo, S. R. Summerfelt, T. San, and J. Kim, "Effect of film thickness on the ferroelectric and dielectric properties of low-temperature (400°C) $\text{Hf}_{0.5}\text{Zr}_{0.5}\text{O}_2$ films," *Appl. Phys. Lett.*, vol. 112, no. 17, Apr. 2018, Art. no. 172902.
- [28] H. J. Kim et al., "Grain size engineering for ferroelectric $\text{Hf}_{0.5}\text{Zr}_{0.5}\text{O}_2$ films by an insertion of Al_2O_3 interlayer," *Appl. Phys. Lett.*, vol. 105, no. 19, Nov. 2014, Art. no. 192903. doi: 10.1063/1.4902072.
- [29] L. Xu, T. Nishimura, S. Shibayama, T. Yajima, S. Migita, A. Toriumi, "Kinetic pathway of the ferroelectric phase formation in doped HfO_2 films," *J. Appl. Phys.*, vol. 122, no. 12, p. 124104, Sep. 2017, doi: 10.1063/1.5003918.
- [30] M. Kao et al., "Variation Caused by Spatial Distribution of Dielectric and Ferroelectric Grains in a Negative Capacitance Field-Effect Transistor," in *IEEE Transactions on Electron Devices*, vol. 65, no. 10, pp. 4652-4658, Oct. 2018, doi: 10.1109/TED.2018.2864971.
- [31] Y. Lin et al., "Effect of Polycrystallinity and Presence of Dielectric Phases on NC-FinFET Variability," 2018 IEEE International Electron Devices Meeting (IEDM), San Francisco, CA, 2018, pp. 9.4.1-9.4.4, doi: 10.1109/IEDM.2018.8614704.
- [32] Y. Liu and P. Su, "Variability Analysis for Ferroelectric FET Nonvolatile Memories Considering Random Ferroelectric-Dielectric Phase Distribution," in *IEEE Electron Device Letters*, vol. 41, no. 3, pp. 369-372, March 2020, doi: 10.1109/LED.2020.2967423.
- [33] Koufos, K., Dettmann, C.P. Distribution of Cell Area in Bounded Poisson Voronoi Tessellations with Application to Secure Local Connectivity. *J Stat Phys* 176, 1296–1315 (2019). https://doi.org/10.1007/s10955-019-02343-y.
- [34] J.-S. Ferenc and Z. N'eda, "On the size distribution of Poisson Voronoi cells," *Physica A: Statistical Mechanics and its Applications*, vol. 385, no. 2, pp. 518–526, Nov. 2007, doi:10.1016/j.physa.2007.07.063.
- [35] MATLAB version: R2016a. [Online] Available: mathworks.com.
- [36] Sentaurus TCAD, Synopsys, Inc., Mountain View, CA, USA, 2017. [Online] Available: http://www.synopsys.com
- [37] Bo Jiang, Zurcher, Jones, Gillespie and Lee, "Computationally Efficient Ferroelectric Capacitor Model For Circuit Simulation," 1997 Symposium on VLSI Technology, Kyoto, Japan, 1997, pp. 141-142, doi: 10.1109/VLSIT.1997.623738.
- [38] M. Hoffmann et al "Demonstration of High-speed Hysteresis-free Negative Capacitance in Ferroelectric $\text{Hf}_{0.5}\text{Zr}_{0.5}\text{O}_2$," 2018 IEEE International Electron Devices Meeting (IEDM), San Francisco, CA, 2018, pp. 31.6.1-31.6.4, doi: 10.1109/IEDM.2018.8614677.